

Superconductivity of bulk MgB_2 + *nano(n)*-SiC composite system: A high field magnetization study

Arpita Vajpayee^{1,2}, V. P. S. Awana^{1,*}, G. L. Bhalla² and H. Kishan¹

¹Superconductivity and Cryogenics Division, National Physical Laboratory, Dr K.S. Krishnan Road, New Delhi-110012, India

²Department of Physics and Astrophysics, University of Delhi, New Delhi-110007, India

Abstract

We study the effect of *nano(n)*-SiC addition on the crystal structure, critical temperature (T_c), critical current density (J_c) and flux pinning in MgB_2 superconductor. X-ray diffraction patterns show that all the samples have MgB_2 as the main phase with very small amount of MgO, further with *n*-SiC addition the presence of Mg_2Si is also noted and confirmed by SEM & EDS. The T_c value for the pure MgB_2 is 18.9K under 8 Tesla applied field, while is 20.8K for the 10-wt % *n*-SiC doped sample under the same field. This points towards the increment in upper-critical field value with *n*-SiC addition. The irreversibility field (H_{irr}) for the 5% *n*-SiC added sample reached 11.3, 10 and 5.8 Tesla, compared to 7.5, 6.5, and 4.2 Tesla for the pure MgB_2 at 5, 10 and 20K respectively. The critical current density (J_c) for the 5-wt % *n*-SiC added sample is increased by a factor of 35 at 10K and 6.5 Tesla field and by a factor 20 at 20K and 4.2 Tesla field. These results are understood on the basis of superconducting condensate (sigma band) disorder and ensuing intrinsic pinning due to B site C substitution clubbed with further external pinning due to available *n*-SiC/ Mg_2Si pins in the composite system.

Key Words: MgB_2 superconductor, nano-particle doping, Flux pinning, Critical current density

* Corresponding author: e-mail: awana@mail.nplindia.ernet.in

Introduction

MgB₂ superconductor has been regarded as a promising material for practical applications at around 20K because of its high critical temperature (T_c), large coherence length (ξ), simple crystal structure, low material cost, high critical current density (J_c) and weak-link-free grain coupling [1,2]. Extensive research has been done on the fabrication of this superconductor in various sample forms, such as polycrystalline bulk, single crystals, metal clad tapes and wires, and thin and thick films [3-5]. For most of the practical applications high critical current density (J_c) in the presence of magnetic field along with high upper critical field (H_{c2}) and high irreversibility field (H_{irr}) are required. J_c of undoped MgB₂ is high enough at low magnetic fields for practical application, however, J_c drops rapidly with increasing magnetic field due to low H_{c2} and lack of the effective pinning sites in MgB₂. Therefore the improvement of J_c under magnetic field is indispensable for development of MgB₂ material for magnet applications. An effective way to improve the flux pinning is to introduce the flux pinning centers into MgB₂ through the dopant having size comparable to the coherence length (of the order of few *nm*) of MgB₂.

It has already been established by now that moderate impurity doping in MgB₂ is effective to increase J_c through introduction of flux pinning centers and/or enhancement of H_{c2} [6-14]. Out of various elements and compounds being doped in MgB₂, the carbon-containing compounds such as SiC, C and B₄C had been found to be more effective. Here, we are reporting the effect of *nano*-SiC addition on the superconducting properties of MgB₂ in high magnetic fields. We found that addition of *n*-SiC into MgB₂ helped in significantly enhancing the J_c and H_{c2} in high fields with only slight reduction of T_c . This is due to the co substitution of broken *n*-SiC for B in MgB₂ lattice inducing intra-grain defects clubbed with high density of nanoinclusions as effective pinning centers. *Nano*-SiC doping is known to enhance both H_{c2} and flux pinning through multiple scattering channel [15]. In the current article, we revisit the MgB₂+*nano*(*n*)-SiC composite system, and compare our results with the existing literature. Recently in ref. 16, we reported the low field (< 7 Tesla) magnetization of some of the presently studied MgB₂+*nano*(*n*)-SiC

samples at 10 and 20K only, and inter-compared the same with $\text{MgB}_{2-x}\text{C}_x$. This was to highlight the role of C in performance of MgB_2 superconductor. In present article we are reporting the detailed high field (up to 14 Tesla) spectacular superconducting performance of though the same system but at various temperatures of 5, 10 and 20K and for a complete series of samples. Further the important superconducting parameter H_{irr} (irreversibility field), which could not be seen in earlier [16] study due to limitation of the applied field, is achieved in the present study. Further it is observed that high field (up to 14 Tesla) performance of $n\text{-SiC}$ added MgB_2 is more spectacular than the low field studies. Our results clearly substantiate the view that the *nano*-SiC addition improves profoundly the high field superconducting performance of MgB_2 superconductor.

Experimental details

Our polycrystalline $\text{MgB}_{2-n}\text{SiC}_x$ ($x = 0, 3\%, 5\%, 7\% \text{ \& } 10\%$) samples were synthesized by solid-state reaction route. The Mg powder used is from *Reidel-de-Haen* and amorphous B powder is from *Fluka* (of assay 95-97%). The $n\text{-SiC}$ powder is from Aldrich having average particle size (APS) of 5-12 nm. For synthesis the samples, the stoichiometric amounts of ingredients were ground thoroughly, palletized using hydraulic press and put in a tubular furnace at 850°C temperature under the flow of argon gas at ambient pressure. This temperature was hold for 2.5 hours, and subsequently naturally cooled under the same atmosphere of argon to room temperature. The X-ray diffraction pattern of the compound was recorded by using CuK_{α} radiation. The scanning electron Microscopy (*SEM*) studies are carried out on these samples using a Leo 440 (Oxford Microscopy: UK) instrument. The magnetoresistivity, $\rho(T)H$, was measured with H applied perpendicular to current direction, using four-probe technique. The magnetization measurements were carried out on *Quantum Design PPMS*, equipped with *VSM* attachment.

Results and Discussions

The x-ray diffraction (XRD) patterns of $\text{MgB}_2:n\text{-SiC}_x$ ($x = 0\%, 3\%, 5\%, 7\% \text{ \& } 10\%$) are shown in fig. 1. In case of pure MgB_2 all characteristic peaks are obtained and their respective indexing is shown in the figure itself. The structure of MgB_2 belongs to space group $P6/mmm$. It can be seen that all doped samples along with the undoped exhibit well developed MgB_2 phase, with only a small amount of MgO present, which is marked by symbol 'o' in fig. 1. The presence of small quantity of MgO being present with MgB_2 main phase is consistent with earlier reports on similar samples [17-19]. No other impurity phases like Mg_2C_3 and MgB_2C_2 are detected.

As we go on increasing the added $n\text{-SiC}$ content in $\text{MgB}_2:n\text{-SiC}_x$, the presence of Mg_2Si (*) and unreacted SiC (+) is noticed. At lower doping level ($x < 7\text{wt}\%$) the sample consist of a major phase of MgB_2 with minority phase of Mg_2Si and as we increase ($x \geq 7\text{wt}\%$) the doping level of $n\text{-SiC}$, the amount of this non-superconducting phase was increased. In particular for $\text{MgB}_2:n\text{-SiC}_x$ ($x = 7\% \text{ \& } 10\%$), the $\{hkl\}$ planes $\{111\}$, $\{220\}$ and $\{400\}$ of the Mg_2Si are noticed clearly in Fig.1. Presence of Mg_2Si has earlier been seen in a recent report [20]. As far as the majority MgB_2 phase is concerned, the peak situated between $2\theta = 33^\circ$ and $2\theta = 34^\circ$ shifts towards the higher 2θ values with increasing x , indicating the contraction in a -axis in crystal lattice. The lattice parameters, ' a ' and ' c ', of the hexagonal AlB_2 type structure of MgB_2 are calculated using these peak shifts, and their variation is tabulated in Ref. [16]. The decrease in ' c ' parameter with increasing x (content of $n\text{-SiC}$) is relatively small as compared to ' a ' parameter. The variation in ' a ' parameter indicated the partial substitution of B by C [21,22].

The grains morphology of pure and $10\text{wt}\%-n\text{SiC}$ added MgB_2 is shown in Fig. 2. The pristine MgB_2 grains are of average size with in less than a micron, also seen are some porous/ MgO insulating white regions, see Fig. 2(a). The presence of Mg_2Si can be noticed in $10\text{wt}\%-n\text{SiC}$ added MgB_2 as large spherical white regions in the MgB_2 matrix along

with smaller insulating MgO. The elemental analysis of these micrographs showed the presence of Si in 2(b) but not in 2(a). This is consistent with the fact that unreacted free Si is present in n -SiC doped samples to form the desired Mg_2Si phase, being seen in XRD in Fig. 1. Though, all the elements being present in MgB_2 or n -SiC doped samples such as Mg, B, and O in former and in addition Si, and C in later are seen in EDS, the actual percentage ratio is not determined because of very light element Boron and Carbon in comparison to others. The sensitivity of SEM is known to be relatively poor for lighter elements such as B, C and O.

Fig. 3 shows the resistance versus temperature curves under magnetic field $R(T)H$ up to 8 Tesla for the undoped, 5% n -SiC and 10% n -SiC doped samples. The transition temperature (T_c) for the pure sample is 38.1K in zero applied field. For the 10 wt% n -SiC added sample T_c decreased to 34.5K in zero applied field. Further, it is noted that the $R(T)$ curves for the doped samples shifted with increasing magnetic field much more slowly than the pure one. The T_c value for the pure MgB_2 is 18.9K for 8 Tesla applied field while is 20.8K for the 10-wt % n -SiC doped sample under the same field.

A further important point is that the nominal resistance of these samples is very different, $R(40\text{K})$ being $290\ \mu\Omega$ for the undoped sample, $490\ \mu\Omega$ for 5 wt % and $800\ \mu\Omega$ for the 10 wt % n -SiC doped sample. This is shown in fig. 4. It refers that the scattering increases with increasing n -SiC content. In inset of fig. 4 the temperature dependence of normalized resistance $R(T)/R(275\text{K})$ is shown for pure and 10% doped sample. The residual resistivity ratio ($\text{RRR} = R_{T275\text{K}}/R_{T\text{onset}}$) values for the pure and 10% SiC doped samples are 3.15 and 1.74 respectively. Both C doping (revealed by contraction in ‘a’ parameter and reduction in T_c) and the inclusion of Mg_2Si (revealed by XRD) can enhance the electron scattering, and hence the decreased RRR values. Further, the higher values of room temperature resistivity for doped samples indicate that the impurity scattering is stronger due to the Carbon substitution at Boron sites. This is in agreement with previous studies on $\text{MgB}_{2-x}\text{C}_x$ systems [21,23]

The variation of upper critical field with respect to reduced temperature is shown in fig. 5, with the help of resistive transitions shown in Fig. 3. All the doped samples show the higher values of critical field in comparison to the pure sample at all the temperatures. The n -SiC reacts with the Mg and releases highly reactive free C on the atomic scale at the same temperature where formation of MgB_2 takes place. Because of the availability of reactive C atom at that time, the C can be easily incorporated into the lattice of MgB_2 and substitute into B sites [24]. The carbon substitution into boron site in lattice is responsible for creating the disorder on the lattice site of boron, which leads to the enhancement in value of upper critical field. Further it is worth mentioning that magnetic field, which is required to destroy the *bulk* superconductivity, is smaller than the magnetic field needed to destroy the *surface* superconductivity, the later is 1.6946 (η) times higher than the former [25,26]. Although this ratio (η) varies with temperature for two- band superconductors but in ref. 25 Denis discussed that at temperature near about the transition temperature (T_c) η takes its highest value that is near about 1.7; overall η takes value from ≈ 1.7 to ≈ 1.64 for temperature variation from T_c to down towards 0K. Therefore, in fig. 5 we are showing the variation of upper critical field H_c , where $H_c = 1.7 \times H$ at $R \rightarrow 0$ ($T \rightarrow T_c$), against the reduced temperature.

The magnetic hysteresis loop for all the doped samples $\text{MgB}_2:n\text{-SiC}_x$ ($x = 0\%$, 3% , 5% , 7% & 10%) are shown in fig. 6 at $T = 5, 10, 20\text{K}$ and under up to 13 Tesla applied field. This figure clearly demonstrates that at $T = 5\text{K}$ the closing of $M(H)$ loop for pure sample is at 7.5 Tesla, while the same is closed at 11.3 Tesla for 5% n -SiC doped sample. This indicates that there is quite an improvement in irreversibility field values by addition of n -SiC in parent compound. The irreversibility fields (H_{irr}) are derived from the fields at which the magnetic hysteresis loop gets nearly closed; with the criterion of giving the $J_c = 100 \text{ A/cm}^2$. To know the effect of doping level of n -SiC on H_{irr} values a plot is drawn in H_{irr} versus x (concentration of n -SiC) and it is shown in fig. 7 at 5K , 10K & 20K . Doping with n -SiC has significantly improved the H_{irr} . At all the temperatures the 5% n -SiC doped samples gives the best value of H_{irr} . The values of H_{irr} for the 5% n -SiC added sample reached 11.3, 10 & 5.8 Tesla, compared to 7.5, 6.5, 4.2 Tesla for the pure one at 5, 10 &

20K respectively. Worth mentioning is the fact that in an earlier preliminary study [16] by some of us, the closing of $M(H)$ loops for n -SiC added samples could not be achieved due to non availability of higher applied fields. The spectacular enhancement in H_{irr} values, being seen in Fig.7, is definitely due to improvement in flux pinning in MgB_2 by the n -SiC doping.

The magnetic J_c for all the samples was calculated from the $M(H)$ loop at 5, 10 & 20K. Fig. 8(a) & 8(b) show the magnetic J_c vs H for all the samples at 20 & 10K respectively. At low fields all the samples attain about 10^5 A/cm² J_c at both the temperatures. Among all the doped samples 5% n -SiC doped sample gives the best performance. For undoped sample J_c drops rapidly in the presence of magnetic field and is almost negligible above 4.2 Tesla and at 6.5 Tesla at 20K and 10K respectively. On the other hand the 5% n -SiC doped sample exhibits the J_c of the order of 10^3 A/cm² at the corresponding fields at both the temperatures. The J_c is 35 times higher than pure one at 10K in 6.5 Tesla field in case of 5% n -SiC doped sample and 20 times higher at 20K in 4.2 Tesla for the same sample. Because of the dual reaction [24], first reaction of n -SiC with Mg forming Mg_2Si and second free C being incorporated into MgB_2 both helps in pinning of vortices and improved superconducting performance. Mg_2Si and excess carbon can be embedded within the grain of MgB_2 as nanoinclusions. Due to the substitution of C at B site the formation of nanodomain structure takes place due to the variation of Mg-B spacing. These nanodomains defects having the size of 2-3 nm can also behave as effective pinning centers. So, the highly dispersed nanoinclusions within the grains and the presence of nanodomain defects are acting as pinning centers and thus resulting in the improved $J_c(H)$ behavior for the n -SiC doped samples.

To confirm the improved flux pinning behavior through SiC doping, the field dependence of normalized flux pinning force ($F_p / F_{p, max}$) is shown in fig. 9(a) & 9(b) at 20K & 10K. The relationship between flux pinning force and critical current density could be described by [27,28]

$$F_p = \mu_0 J_c(H) H \quad (1)$$

Where μ_0 is the magnetic permeability in vacuum. These figures depict a significant improvement in pinning forces by *n*-SiC doping at both the temperatures for fields greater than 2 Tesla. Flux pinning curves for the doped samples are shifted to the right as compared to pure MgB₂. As described earlier the nanoinclusions and nanodomains having the size comparable to coherence length of MgB₂, can work as point pinning centers, causing a shift of the curve in $F_p / F_{p,max}$ vs H curve towards the higher field. It can be seen from fig. 9 that for the 5-wt% *n*-SiC doped sample the peak is much broader than those of other samples, indicating that the highest pinning strength for this sample; this is in confirmation with J_c results. As far as the type of pinning i.e., grain boundary, point defects or order parameter change is concerned; in our case it is seemingly the combination of grain boundary and point defects. The former is due to the presence of grain boundary precipitates of Mg₂Si and later due to inclusions of *n*-SiC. This we presume because the $F_p / F_{p,max}$ vs H peak does not only get broadened (grain boundary pinning) with *n*-SiC addition but there is a slight right direction shift in peak position to higher fields as well [29].

Worth mentioning is the fact that though all *n*-SiC added samples till 10wt% addition are superior than that to the pristine MgB₂, the 5-wt% *n*-SiC added one is the optimum. In our recent another paper [16] in which we discussed about role of carbon in MgB₂ lattice to enhance the flux pinning performance comparatively at lower fields, we found that 7-wt% *n*-SiC added sample of different batch showed the highest improvement in the flux pinning. Therefore, we can say that due to *n*-SiC doping superconducting performance enhances profoundly and the optimum is found between say 3 to 7-wt% additions. The fact is that 5-wt% or 7-wt% amount of *n*-SiC is not the optimum for achieving the best J_c , H_{irr} & H_{c2} ; it all depend on the various other factors like synthesis temperature, heating rate, annealing time, magnetic field and resultant sample quality etc [7,30].

Conclusions

In summary, the effect of *nano* SiC doping on critical temperature (T_c), critical current density (J_c) and flux pinning was investigated under a wide range of magnetic field. We found that a significant flux pinning enhancement in MgB_2 can be easily achieved using *nano* SiC as an additive. The Si and C released from the decomposition of *nano* SiC at the time of formation of MgB_2 formed Mg_2Si and substituted at B sites respectively. The C substitution for B resulted in a large number of intra-granular dislocations and dispersed nanosize impurities, which are both responsible for the significant enhancement in flux pinning.

Acknowledgement

The authors from *NPL* would like to thank Dr. Vikram Kumar (*DNPL*) for his great interest in present work. Mr. A.K. Sood from *SEM* Division of *NPL* is acknowledged for providing us with the *SEM* micrographs. Dr. Rajeev Rawat from *CSR*-Indore is acknowledged for the resistivity under magnetic field measurements. Mr. Kranti Kumar and Dr. A. Banerjee are acknowledged for the high field magnetization measurements. Further *DST*, Government of India is acknowledged for funding the 14 Tesla-PPMS-VSM at *CSR*, Indore. Arpita Vajpayee would like to thank the *CSIR* for the award of Junior Research Fellowship to pursue their *Ph. D* degree.

References

1. Buzea C and Yamashita T 2001 *Supercond. Sci. and Tech.* **14** R115
2. Iwasa Y, Larbalestier D C, Okada M, Penco R, Sumption M D and Xi X 2006 *Trans. Appl. Supercond.* **16** 1457
3. Canfield P C, Bud'ko S L and Finnemore D K 2003 *Physica C* **385** 1
4. Flukiger R, Suo H L, Musolino N, Beneduce C, Toulemonde P and Lezza P 2003 *Physica C* **385** 286
5. Lee S 2003 *Physica C* **385** 31
6. Dou S X, Slotanian S, Horvat J, Wang X L, Zhou S H, Ionescu M, Liu H K, Munroe P and Tomsic M 2002 *Appl. Phys. Lett.* **81** 3419
7. Yeoh W K, Kim J H, Horvat J, Xu X, Qin M J, Dou S X, Jiang C H, Nakane T, Kumakura H and Munroe P 2006 *Supercond. Sci. and Tech.* **19** 596
8. Yamada H, Hirakawa M, Kumakura H and Kitaguchi H 2006 *Supercond. Sci. and Tech.* **19** 175
9. Cheng C H, Zhang H, Zhao Y, Feng Y, Rui X F, Munroe P, Zeng H M, Koshizuka N and Murakami M 2003 *Supercond. Sci. and Tech.* **16** 1182
10. Senkowicz B J, Giencke J E, Patnaik S, Eom C B, Hellstrom E E and Larbalestier D C 2005 *Appl. Phys. Lett.* **86** 202502
11. Wilke R H T, Bud'ko S L, Canfield P C and Finnemore D K 2004 *Phys. Rev. Lett.* **92** 217003

12. Xiang J Y, Zheng D N, Li J Q, Li S L, Wen H H and Zhao Z X 2003 *Physica C* **386** 611
13. Yeoh W K and Dou S X 2007 *Physica C* **456** 170
14. Matsumoto A, Kumakura H, Kitaguchi H and Hatakeyama H 2003 *Supercond. Sci. and Tech.* **16** 926
15. Dou S X, Baccini V, Soltanian S, Klie R, Zhu Y, Wang X L and Larbalestier D C 2004 *J. Appl. Phys.* **96** 7549
16. Awana V P S, Vajpayee Arpita, Mudgel Monika, Rawat Rajeev, Acharya Somobrata, Kishan H, Takayama Muromachi E, Narlikar A V and Felner I 2007 *Physica C* **467** 67
17. Yan S C, Yan G, Lu Y F and Zhou L 2007 *Supercond. Sci. and Tech.* **20** 549
18. Dou S X, Pan A V, Zhou S, Ionescu M, Wang X L, Horvat J, Liu H K and Munroe P R 2003 *J. Appl. Phys.* **94** 1850
19. Dou S X, Pan A V, Zhou S, Ionescu M, Liu H K and Munroe P R 2002 *Supercond. Sci. and Tech.* **15** 1587
20. Dou S X, Yeoh W K, Shcherbakova O, Wexler D, Zhong Y L, Ren M, Munroe P, Chen S K, Tan K S, Glowacki B A and MacManus-Driscoll J L 2006 *Adv. Mater.* **18** 758
21. Bharthi A, Balaselvi S J, Kalavathi S, Reddy G L N, Sastry V S, Hariharan Y and Radhakrishnan T S 2002 *Physica C* **370** 211

22. Avdeev M, Jorgensen J D, Ribeiro R A, Budko S L and Canfield P C 2003 *Physica C* **387** 301

23. Balaselvi S J, Gayathri N, Bharthi A, Sastry V S and Hariharan Y 2004 *Supercond. Sci. and Tech.* **17** 1401

24. Dou S X, Sheherbakova O, Yeoh W K, Kim J H, Soltanian S, Wang X L, Senatore C, Flukiger R, Dhalle M, Husnjak O and Babie E 2007 *Phys. Rev. Lett.* **98** 097002

25. Gorokhov Denis A 2005 *Phys. Rev. Lett.* **94** 077004

26. Lyard L, Samuely P, Szabo P, Klein T, Marcenat C, Paulius L, Kim K H P, Jung C U, Lee H S, Kang B, Choi S, Lee S I, Marcus J, Blanchard S, Jansen A G M, Welp U, Karapetrov G and Kwok W K 2002 *Phys. Rev. B* **66** 180502(R)

27. Martinez E, Mikheenko P, Martinez-lopez M, Millan A, Bevan A and Abell J S 2007 *Phys. Rev. B* **75** 134515

28. Shen T M, Li G, Cheng C H and Zhao Y 2006 *Supercond. Sci. and Tech.* **19** 1219

29. Tarantini C, Aebbersold H U, Bernini C, Braccini V, Ferdeghini C, Gambardella U, Lehmann E, Manfrinrtti P, Palenzona A, Pallecchi I, Vignolo M and Putti M 2007 *Physica C* **463-465** 211

30. Chen S K, Tan K S, Glowacki B A, Yeoh W K, Soltanian S, Horvat J and Dou S X 2005 *Appl. Phys. Lett.* **87** 182504

Figure captions

Figure 1. X-ray diffraction pattern of pure and n -SiC doped samples

Figure 2 (a,b). SEM pictures of Pure MgB_2 & 10-wt% n -SiC added sample

Figure 2(c). EDS pattern of pure MgB_2 and 10-wt% n -SiC added sample. Peaks for different elements are marked.

Figure 3. Superconducting transition zone of Resistance vs Temperature plot under applied magnetic field $R(T)H$ up to 8 Tesla for pure, 5-wt% & 10-wt% n -SiC added samples

Figure 4. Variation of resistance with temperature $R(T)$ plots for Pure, 5% and 10% n -SiC added samples

Figure 5. Upper critical field (H_{c2}) vs normalized temperature plots for $\text{MgB}_2+n\text{-SiC}_x$ $x=0\%$, 3%, 5%, 7% & 10% samples

Figure 6. Magnetization loop $M(H)$ for $\text{MgB}_2+n\text{-SiC}_x$ ($x=0\%$, 3%, 5%, 7% & 10%) up to 13 Tesla field at 5, 10 & 20K

Figure 7. Variation of irreversibility field H_{irr} with respect to n -SiC concentration at 5K, 10K & 20K

Figure 8. $J_c(H)$ plots for $\text{MgB}_2+n\text{-SiC}_x$ samples along with pristine MgB_2 at (a) 20K & (b) 10K

Figure 9. Variation of reduced flux pinning force ($F_p/F_{p,max}$) with magnetic field for $\text{MgB}_2+n\text{SiC}_x$ ($x=0\%$, 3%, 5%, 7% & 10%) at (a) 20K & (b) 10K

Figure 1

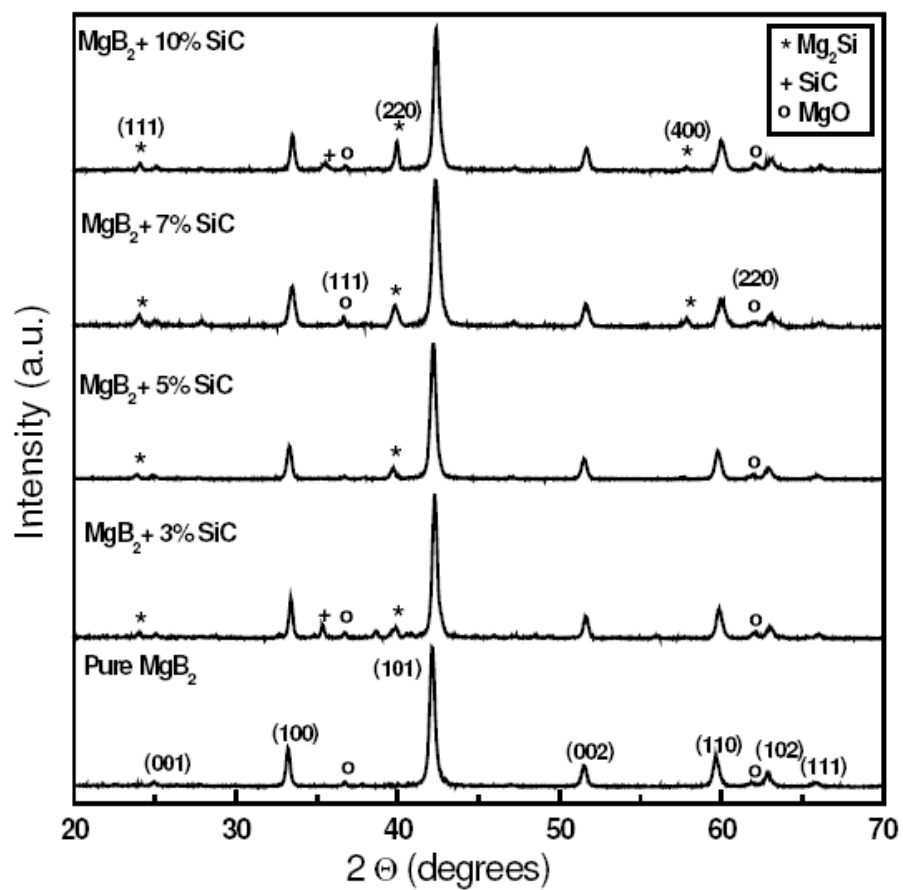


Figure 2(a)

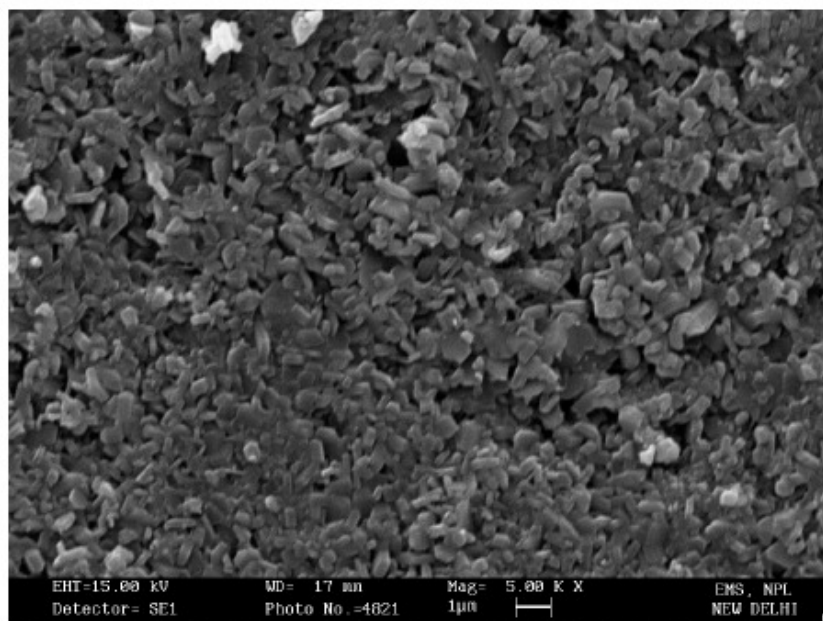


Figure 2(b)

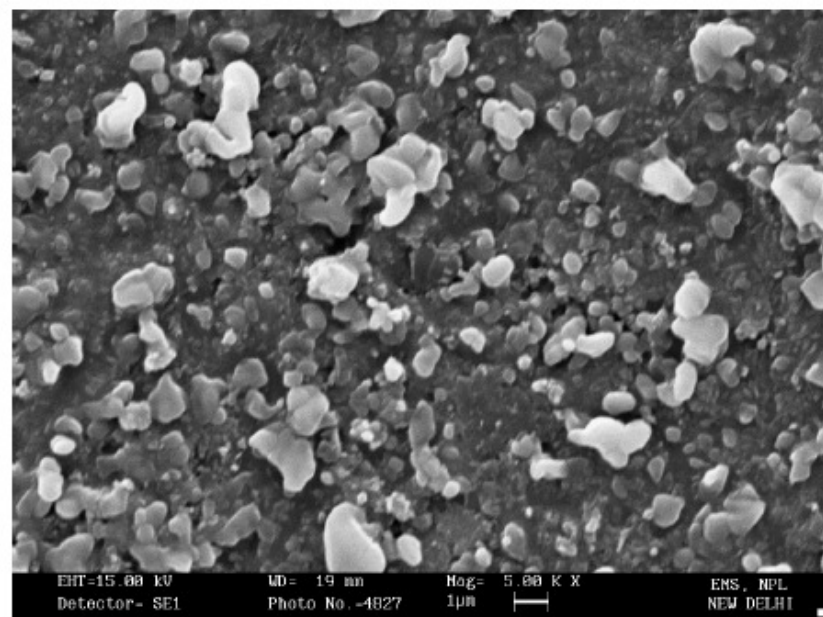


Figure 2(c)

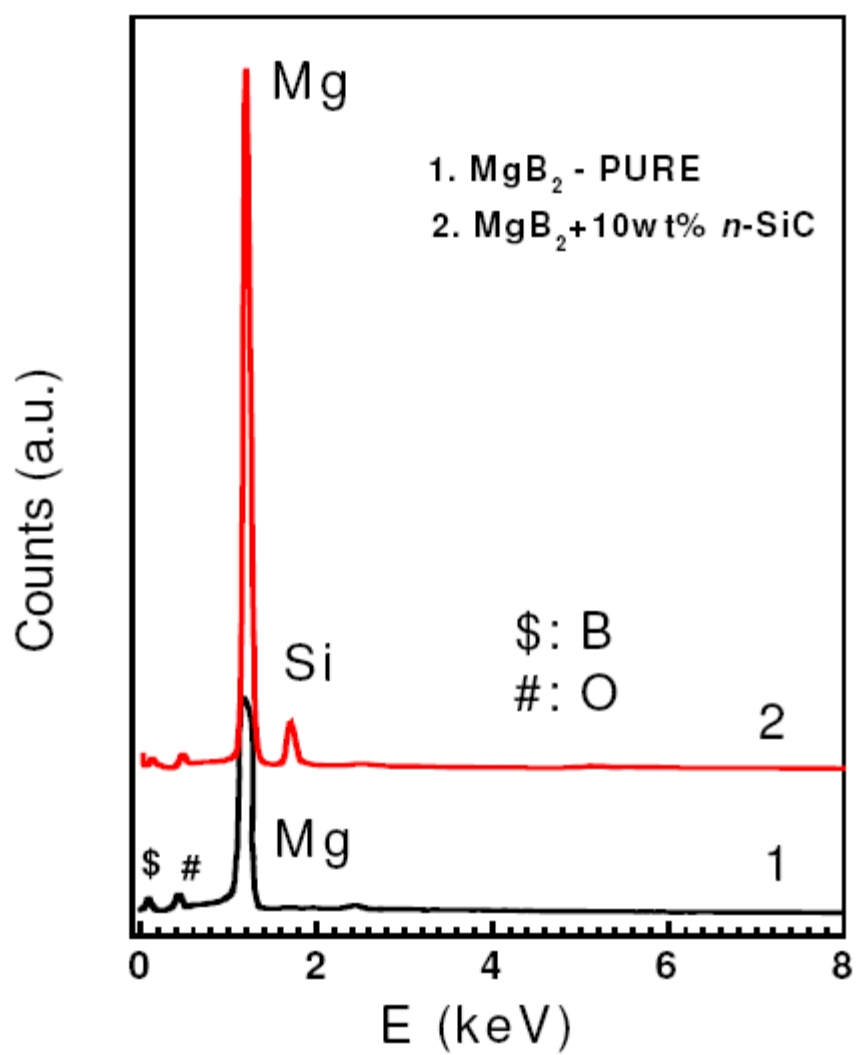


Figure 3

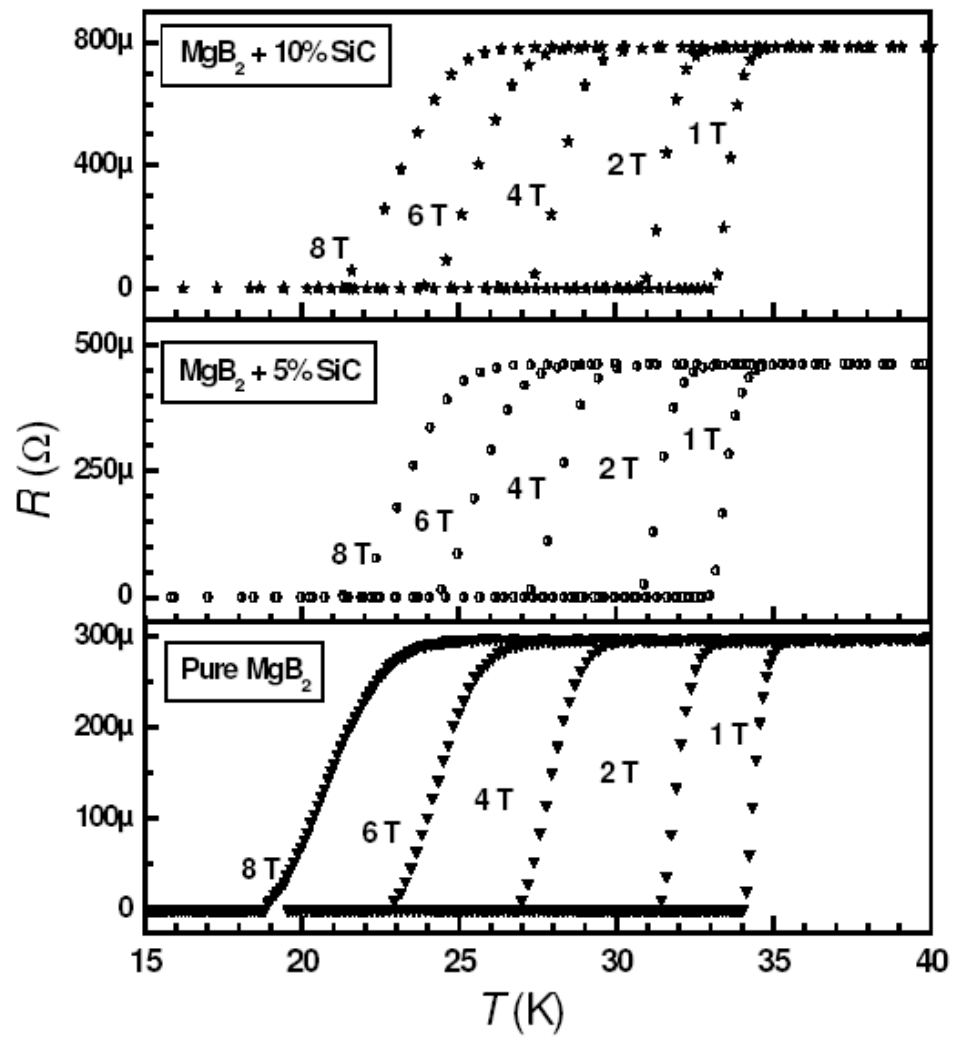


Figure 4

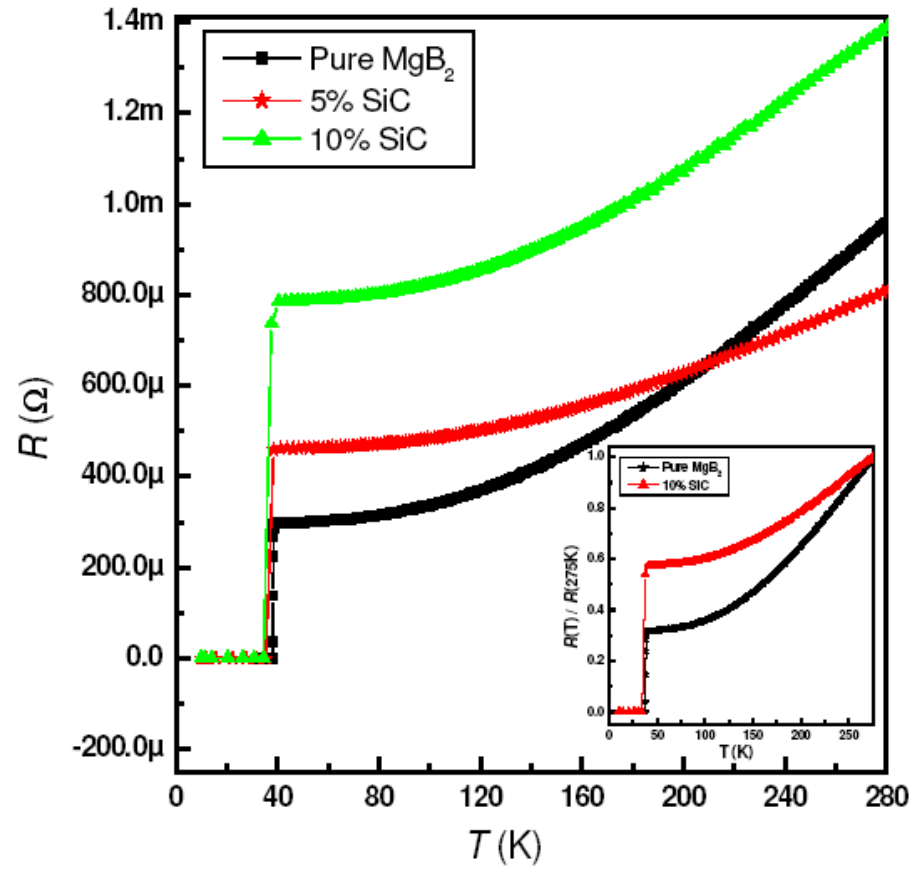


Figure 5

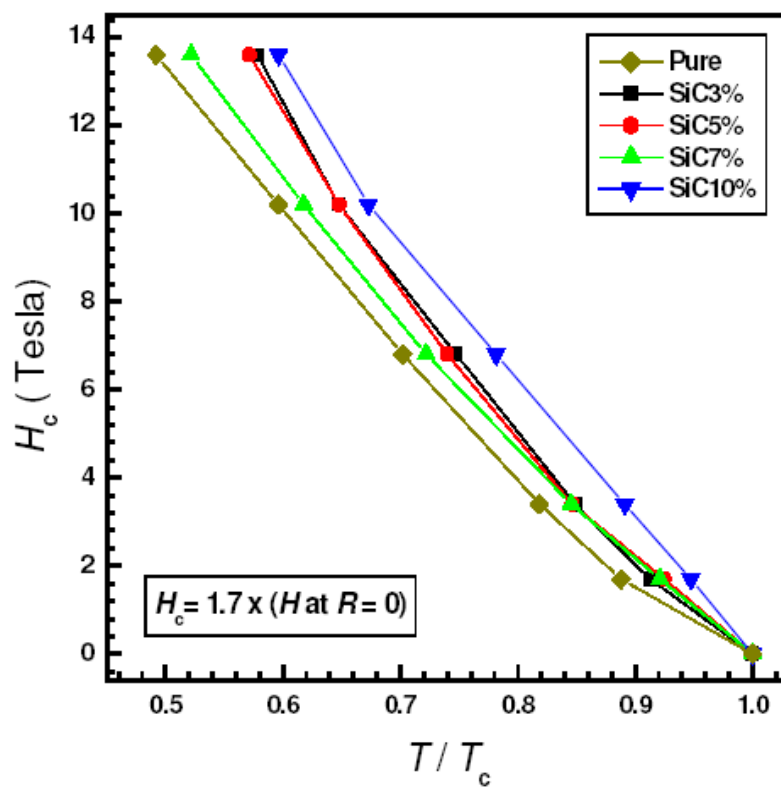


Figure 6

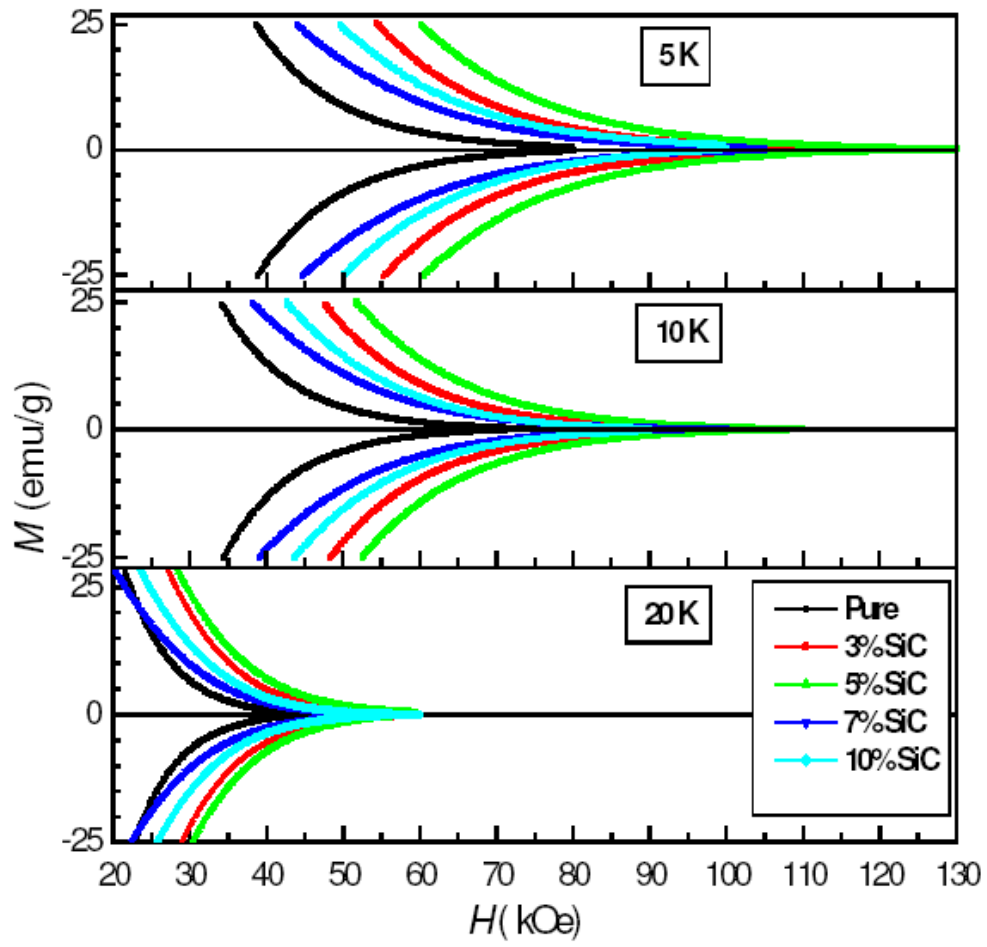


Figure 7

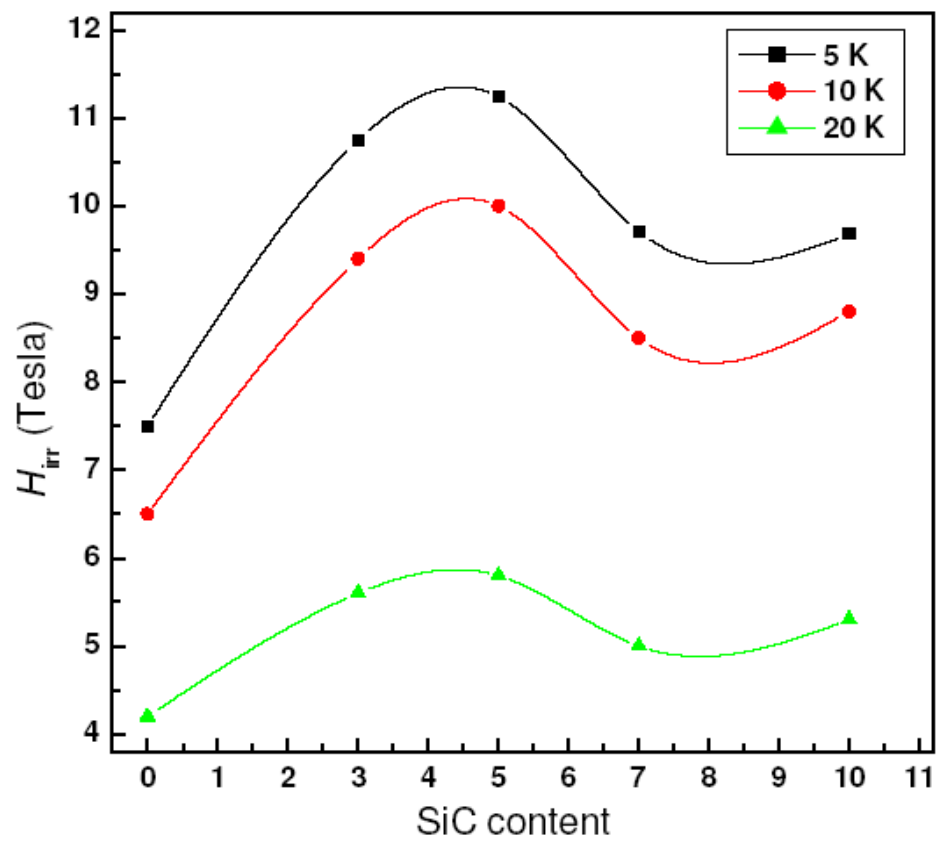


Figure 8 (a) & 8 (b)

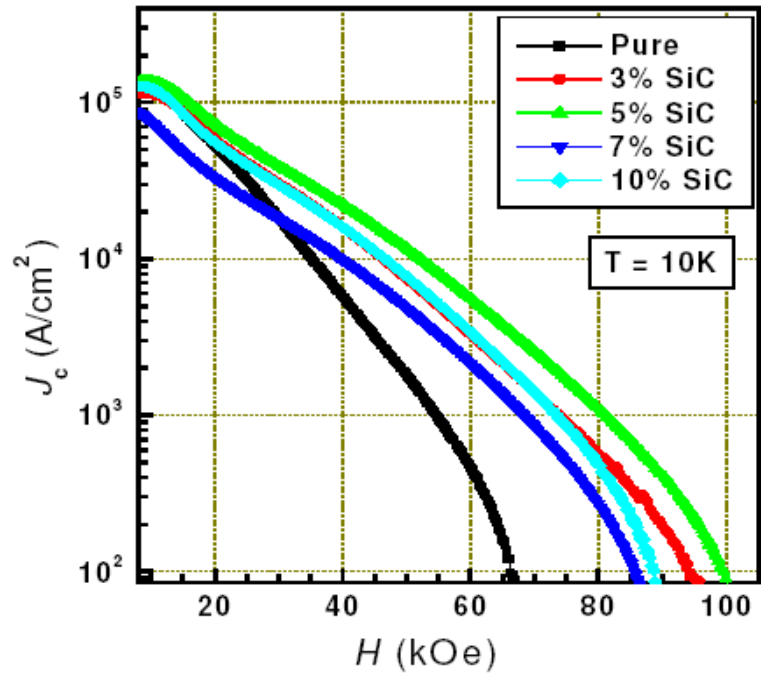
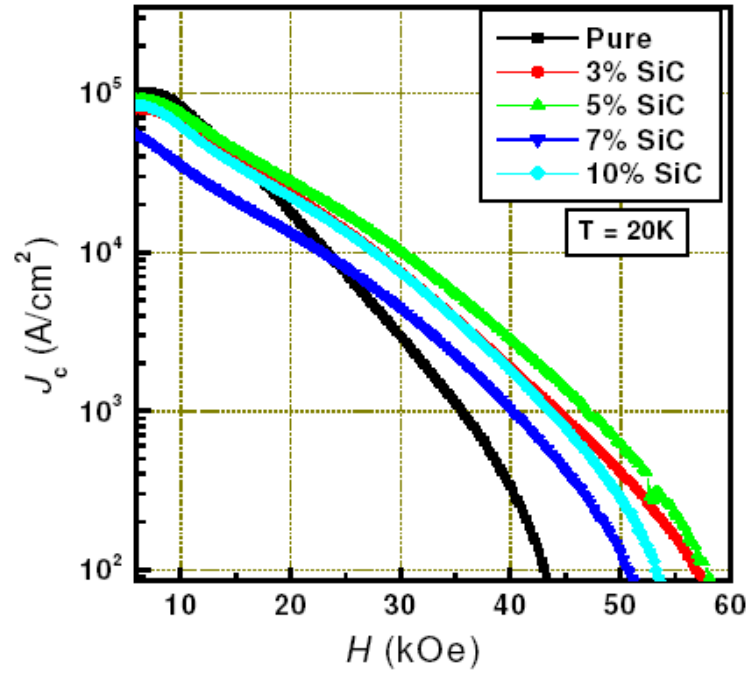


Figure 9(a) & 9(b)

